

ERO modeling of beryllium erosion by helium plasma in experiments at PISCES-B



D. Borodin^{a,*}, D. Nishijima^b, R.P. Doerner^b, S. Brezinsek^a, A. Kreter^a, A. Kirschner^a, J. Romazanov^a, I. Borodkina^{c,a}, A. Eksaeva^{a,c}, E. Marenkov^c, Ch. Linsmeier^a

^aForschungszentrum Jülich GmbH, Institut für Energie- und Klimaforschung – Plasmaphysik, Partner of the Trilateral Euregio Cluster (TEC), 52425 Jülich, Germany

^bCenter for Energy Research, University of California at San Diego, 9500 Gilman Dr., La Jolla, CA 92093-0417, USA

^cNational Research Nuclear University (MEPhI), Kashirskoe sh. 31, Moscow, Russian Federation

ARTICLE INFO

Article history:

Received 18 August 2016

Revised 24 April 2017

Accepted 9 May 2017

Available online 31 May 2017

Keywords:

Beryllium

Erosion

Helium

ERO code

PISCES-B

Spectroscopy

ABSTRACT

The beryllium erosion by helium plasma irradiation is studied at the PISCES-B linear plasma device and interpreted using the accompanying simulations by the ERO code. The influence of plasma conditions and varying negative biasing of the Be plasma target on BeI and BeII absolute line intensities are reproduced in detail by the simulations. The synthetic axial line intensity shapes and line ratios match with experiment. This indicates that atomic data are quite accurate. The initial population state of quasi-metastable ³P level in BeI is found to be MS:GS = 0.33:1 for all conditions. The yields determined by the modeling interpretation are compared to the SDTrimSP code simulations in the binary collision approximation.

© 2017 The Authors. Published by Elsevier Ltd.

This is an open access article under the CC BY-NC-ND license.

(<http://creativecommons.org/licenses/by-nc-nd/4.0/>)

1. Introduction

Reliable data for beryllium (Be) erosion is a key for predictive modeling of ITER first wall duty cycle [2]. Physical sputtering by hydrogenic species plays the main role, however the erosion due to the expected impurities like helium (He) is also of importance. He is of importance not only because it will be a product of fusion, but also because it is proposed to use the He plasma at the starting (low activation) phase of the ITER operation [3]. The 3D Monte-Carlo impurity transport and plasma-surface interaction (PSI) code ERO is often used for ITER predictions [4,5]. Therefore it is of importance to validate both the code and the underlying data (e.g. for physical erosion) at existing devices like PISCES-B [1,10] capable to operate with Be. Recently the ERO code was also extensively applied to various erosion experiments at JET ITER-like wall (ILW) [6,7,8,24] which have led to extensions and refinements of the model and data in ERO. Multiple improvements were implemented including an analytical treatment of the distributions of angles and energies on impact including additional surface biasing [11]. The ERO application to the PSI-2 linear device has contributed in providing the initial angle distributions for physically sputtered

species [12] (for W erosion; operation with toxic Be is not allowed at PSI-2). In parallel the empirical experience at PISCES-B has grown, for instance the indication for a rise of the electronic temperature (mostly a constant axial profile for T_e is assumed) just in front of the target was discovered [9].

In the present work the updated ERO code is applied to the benchmark of physical sputtering data by experiments at PISCES-B, the only alternative to JET for plasma operation with Be. PISCES-B provides unique opportunities for Be spectroscopy like continuous plasma operation and a possibility to observe the triplet 332 nm line allowing to characterize the **BeI 1s²2s2p ³P** quasi-metastable state (MS) population [17]. This particular study is aimed in understanding of the pure physical sputtering of Be by He plasma irradiation which allows excluding any **Be-D_x** molecule release and respective uncertainties.

The experiment has provided an extensive spectroscopy and weight loss benchmark data. 2 BeI (triplet and singlet) and 2 BeII axial line intensity profiles were obtained in He plasmas in the vicinity of the Be target. The negative target biasing was scanned (from −50 to −125 V) in 3 plasma conditions to study the influence of the sputtering ions impact energy. To provide an independent measurement several target weight loss measurements were performed at similar conditions.

* Corresponding author.

E-mail address: d.borodin@fz-juelich.de (D. Borodin).

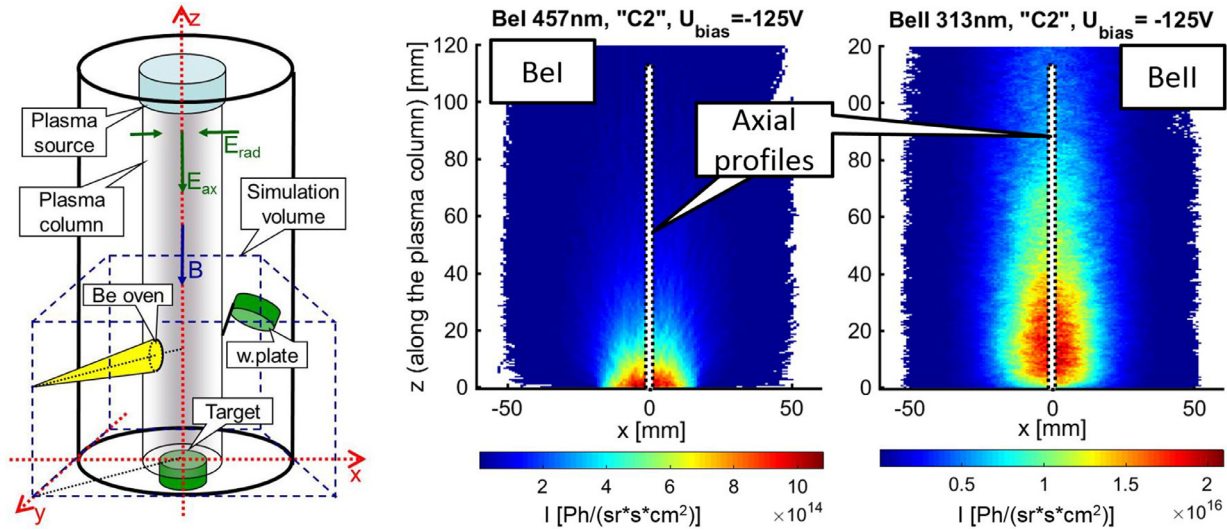


Fig. 1. The illustration of the PISCES-B linear device including ERO simulation volume and coordinate system (left). Be effusion cell (“oven”) and witness plate (“w.plate”) are shown though they are not in use in the experiment discussed in the present paper. ERO simulated light emission of BeI and BeII are shown (middle and right), the position of the axial profiles measured in experiment and synthesized by ERO are shown.

The physical sputtering yields $Y_{Be \leftarrow He}(E_{in})$ for Be erosion by He ions as a function of impact energy E_{in} based on the SDTrimSP code simulations in the binary collision approximation (BCA) in a form of Eckstein’2007 fitting formula [14] are compared to the absolute values resulting from the experiment with the ERO modeling interpretation.

2. Experiment and benchmark data for the Be erosion modeling

The illustration of the PISCES-B linear device is given in Fig. 1 (left). The Be target is positioned inside the plasma column with the surface perpendicular to the axial B-field. The spectroscopic measurements during Be exposure to the He plasma with varying conditions and external target biasing were dedicated for interpretation using the ERO modeling. ERO simulates the Be erosion, deposition and reflection as well as the local transport in the vicinity of the target. In Fig. 1 (right) one can see the ERO simulated side views of neutral BeI and ionized BeII emission. They are essentially different: the pattern of BeI is very much affected by the initial angle distribution of the sputtered Be, whereas BeII is more elongated along the device axis due to confinement of the ions by the axial B-field. Still, the plasma flow clearly pulls them back to the target. The light emission plume of eroded Be is characterized by axial line intensity profiles which are also useful for comparison of the experiment with the simulations.

The incidence of sputtering He ions is nearly normal to the target with a surface perpendicular to the electric field, because the B-field in PISCES-B is relatively weak ($B = 0.0152T$). The sheath (and less significant pre-sheath) electric field pulling the ions to the target is dominating over other effects on the ion movement direction and their energy on impact with the surface in particular in the case of an additional negative biasing applied to the target like in the considered experiment. The sputtering yields at normal incidence are mostly dependent [14] on the material parameters like surface binding energy, lattice configuration and displacement energy etc., and the mass and the incidence energy of the sputtering ions E_{in} . The latter is determined by the biasing mentioned with the potential U_{bias} as $E_{in} = Z_{ion}^*(U_{plasma} - U_{bias})$, where U_{plasma} is the plasma potential. In some cases (mass loss experiment, Section 4) U_{plasma} was measured by a Langmuir probe, but in case this was not available, it is assumed to be $U_{plasma} \sim T_e$.

The latter assumption is based on both empirical and modeling experience at PISCES-B and is indirectly justified to be quite adequate by the good reproduction of the erosion dependence on the target biasing by the modeling (see Fig 5, top).

The scans of the target biasing (E_{in}) were performed in three plasma conditions (Table 1). The electron density n_e and temperature T_e were measured by the reciprocating Langmuir probe at the axis at 15 cm distance from the target surface. It should be noted n_e decreases towards the target down to ~50% from the upstream value on a distance of about ~15 cm [15]. T_e is assumed to be constant in the axial direction. The plasma column has a width of about 5 cm with a Gaussian radial profile of n_e and a somewhat flatter (similar to pedestal) radial profile for T_e . The target sample is a disk with a radius of 11 mm fixed by the clamping ring also made of Be which increases the total radius up to 18 mm.

Three He plasma exposures with the mass loss measurements at plasma conditions somewhat different to the ones in the spectroscopic measurements were performed to provide an independent yield measurement for the benchmark. ERO modeling accounts for plasma conditions at each considered case and allows to relate the measurements with each other.




It should be noted, that it is our general approach to keep all the modeling assumptions exactly the same in all the simulations except the plasma and target biasing parameters, which were varied in experiment to study their influence or because of the experimental programme history (weight loss cases). The sensitivity studies made for e.g. T_e near the target or metastable level population (see below) were involving these parameters only. Of course the variation of for instance plasma density affects not only the sputtering flux, but also e.g. the emissivity of Be species, however ERO is supposed to account for the respective affects and their interplay according to the build-in models and underlying data (e.g. rates for atomic processes).

3. Spectroscopy: simulations and experiment

It was of importance to reproduce the shape of the experimental profiles and the line ratios, because it validates the feasibility of the local transport simulations and atomic data used. Fig. 2 shows a typical example for condition ‘C2B3’ (Table 1). The agreement for other conditions is very similar. The decay of BeI lines with a growing distance from the target is determined to a certain ex-

Table 1

The plasma and biasing conditions in the experiment and the respective reference names used in the following figures.

Plasma	At axis, z=150mm	Biasing	ERO 'name'
'C1' 	$n_e=12 \cdot 10^{12} \text{cm}^{-3}$ $T_e=4.8 \text{eV}$ $P_{\text{neutrals}}=7.3 \text{mTorr}$ $B=0.0152 \text{T}$	'B1' V=-50V	1) 'C1B1'
		'B2' V=-75V	2) 'C1B2'
		'B3' V=-100V	3) 'C1B3'
		'B4' V=-125V	4) 'C1B4'
'C2' 	$n_e=6.5 \cdot 10^{12} \text{cm}^{-3}$ $T_e=7.7 \text{eV}$ $P_{\text{neutrals}}=3.8 \text{mTorr}$ $B=0.0152 \text{T}$	'B1' V=-50V	5) 'C2B1'
		'B2' V=-75V	6) 'C2B2'
		'B3' V=-100V	7) 'C2B3'
		'B4' V=-125V	8) 'C2B4'
'C3' 	$n_e=4.0 \cdot 10^{12} \text{cm}^{-3}$ $T_e=11.5 \text{eV}$ $P_{\text{neutrals}}=2.5 \text{mTorr}$ $B=0.0152 \text{T}$	'B1' V=-50V	9) 'C3B1'
		'B2' V=-75V	10) 'C3B2'
		'B3' V=-100V	11) 'C3B3'
		'B4' V=-125V	12) 'C3B4'

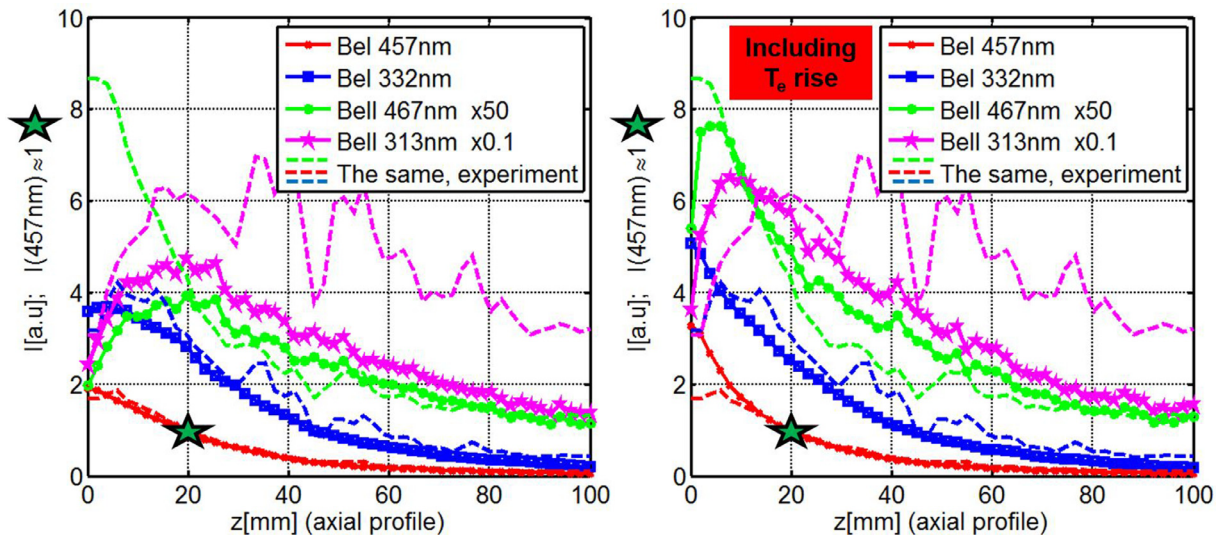


Fig. 2. The axial line intensity profiles of various BeI and BeII lines measured at PISCES-B during the Be target exposure to He plasma and the corresponding ERO simulations (dashed lines of the same color). Both the experimental and the simulated profiles are normalized to the intensity of 457 nm BeI line at the location marked by the star, which is used in the following figures for the absolute value comparison. Plasma condition 'C2' (see Table 1).

tent by ionisation, however it is much more affected by the angular distribution just after the sputtering, which determines how much neutrals leave the plasma volume to the sides. The perfect match between triplet and singlet lines in BeI demands metastable population tracking discussed below. The relatively good match of BeI to BeII ratio confirms the reasonability of plasma parameters and atomic data. The best match of BeII decay far from the target demands an additional assumption of a cut-off angle (COA) in the angular distribution of the sputtered Be atoms. This allows to get a larger BeII fraction far away from the target. It should be noted that the noise and error bars for BeII lines (in particular 313 nm) are higher than for BeI. Optimal COA determination is not very precise as the most critical part of the axial profile for that is the decayed signal far away from the target. Obviously it is mostly affected by noise and background subtraction assumptions. COA = 30° works well for conditions "C1" and "C2", whereas

the match of "C1" remains reasonable even in at COA = 10°. The physics behind the COA is discussed below.

It was shown earlier in [9] that the BeII and He line ratios as well as Langmuir probe measurements indicate the rise of a T_e towards the target in its very vicinity by a factor of about 1.5–3 which depends on the pressure of neutral gas filling the PISCES-B volume. This effect was introduced for sensitivity study in ERO as a correction factor based on BeII line ratio measurements interpreted with the help of ADAS'96 [16] data. Fig. 2, right shows that the assumption of this rise improves agreement for BeII lines, however the profile agreement for BeI just in front of the target gets somewhat worse. This may be explained for instance if the radial distribution of this rise is not constant.

The main aim of the present paper, which is to determine the absolute sputtering yields from spectroscopy and values just in front of the target, are fogged by the described uncertainty. The

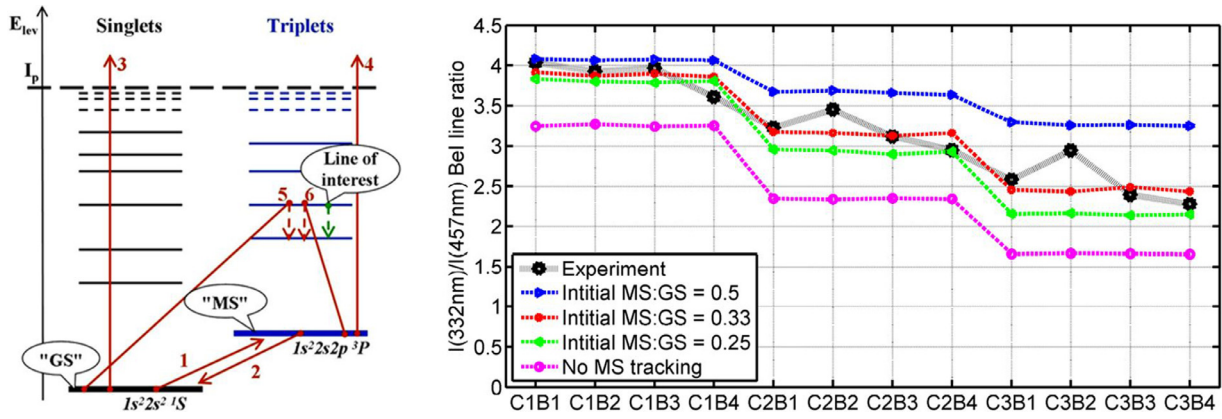


Fig. 3. The triplet (332 nm) to singlet (457 nm) line ratios in BeI as obtained in the experiment (black stars) or simulated by ERO using various assumptions about the initial population just after sputtering or with switched off MS tracking.

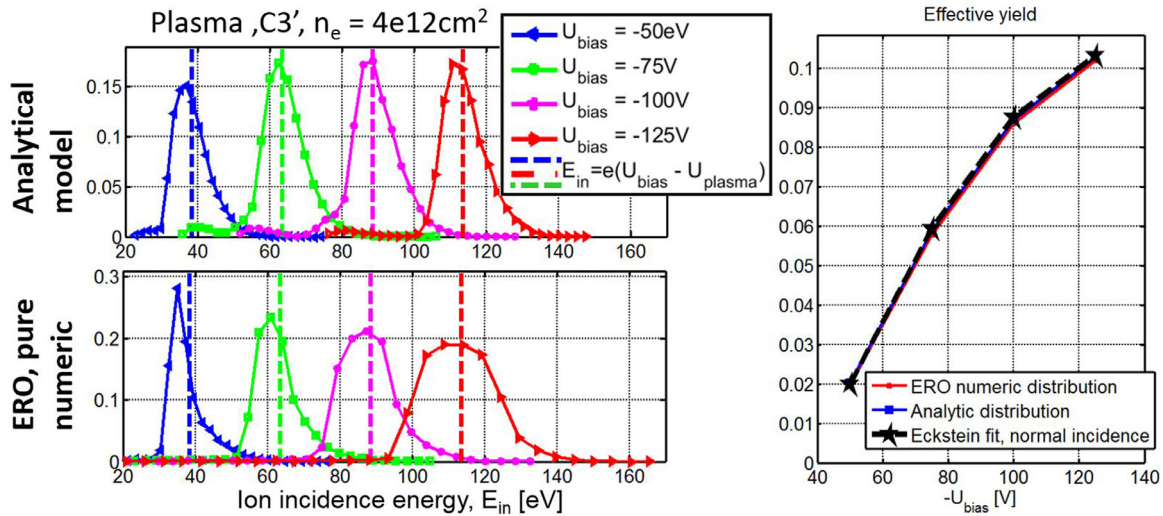


Fig. 4. The energy distributions of the sputtering ions for the condition 'C3' (see Table 1) generated by the pure numeric (special ERO run) and the analytic approaches (left) and the respective effective sputtering yields (right). The dashed lines indicate the characteristic impact energies for He^+ ions equal to $U_{\text{bias}} - U_{\text{plasma}}$.

simulations have shown that the part of the BeI 457 nm line profile between $z = 20 \text{ mm}$ and $z = 60 \text{ mm}$ is much more suitable for integration of absolute intensities, because its shape is independent of the assumptions concerning T_e rise and COA. The integration along the 40 mm of profile length increases the signal to noise ratio. In all figures below all values including the line ratios are produced on the basis of the values integrated in the explained way for both BeI lines.

To get the nearly perfect match for relative intensities of the singlet 457 nm and triplet 332 nm lines one can see in Fig. 3 (left), the MS tracking should be used [17]. In general words the tracking of the BeI $1s^2 2s 2p^3 P$ population (this quasi-MS state is the lowest in the triplet system) allows ERO to follow the relative total population of all triplet states against the total population of the singlet system. It can be shown that relaxation between the systems due to intercombinational transitions is much slower than inside each system. Naturally, the contributions to the spectral line photon efficiency coefficients [16] from the states belonging to the same spin are usually the largest. Sputtered particles leave the surface with an unknown initial internal state, which however can be determined from the line ratio mentioned. In Fig. 3, ERO simulations based on various assumptions are presented alongside with the experiment for all experimental conditions available (Table 1). The initial population of MS:GS=0.33 seems to fit best (Fig. 3, right) independent of plasma conditions and surface biasing. The

quantum mechanical reasons for this interesting fact are not yet studied, however this is out of the scope of the present paper.

The number of photons emitted by each Be species depends on the above described factors whereas their amount is proportional to the gross erosion fully determined in the case at hand by physical sputtering. This process is known to depend on the angle and energy [7] of the sputtering ions, however, due to the nearly normal incidence of sputtering He^+ ions in PISCES-B, the angular factor in the Eckstein'2007 formula for the sputtering yields [14] is equal to unity. The energy of incidence E_{in} distribution can be of importance also, therefore in the case at hand it was investigated (Fig. 4, left) by dedicated ERO simulations as well as an analytical approach [11]. These approaches do not agree fully with each other, in particular in the high density condition "C1", which is more difficult for ERO from a numerical point of view due to higher collisionality. However, the main outcome is absolutely the same: the E_{in} distribution is relatively narrow around the average value determined by biasing. Fig. 4, right shows that the effective yield averaged by any of these distributions nearly exactly matches the normal incidence yield, thus the energy distribution can be neglected.

The intensities integrated between $z = 20 \text{ mm}$ and $z = 60 \text{ mm}$ mimic the absolute sputtering yields (Be light emission is directly proportional to the flux of the eroded species and thus, to the assumed sputtering yield). Fig. 5 presents the ERO simulations in

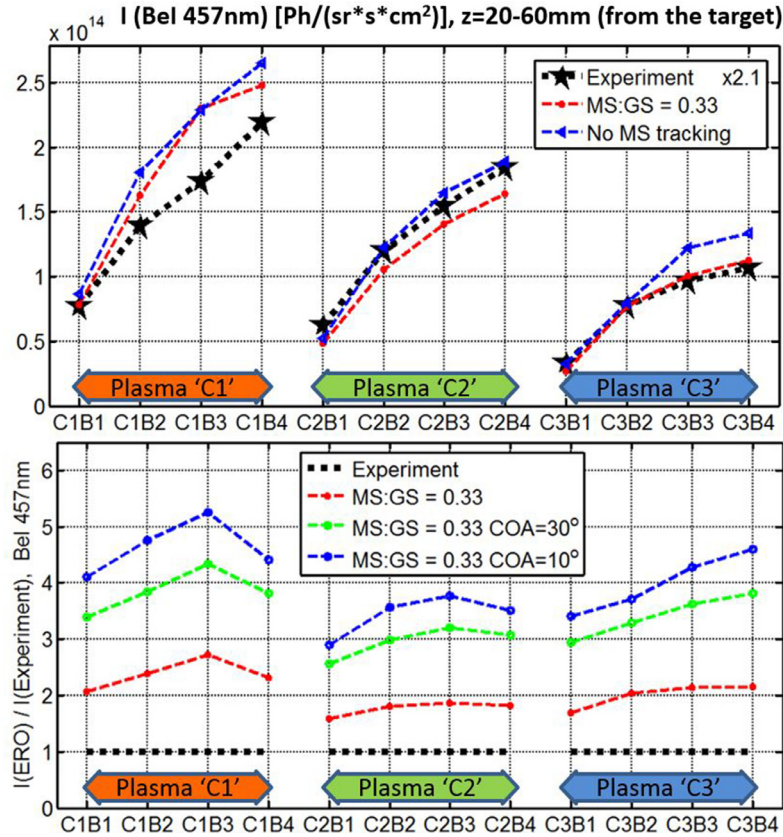


Fig. 5. Integrated light emission values near the Be target at various plasma and biasing conditions (Table 1). The absolute intensity values ERO with and without MS-tracking and the experimental ones (top). The ratios to the experimental values of simulations with various cut-off angle assumptions (bottom).

Table 2

Three experiments at PISCES-B with Be target irradiation by He plasma and various estimations (or ERO simulations) for sputtering yields. ERO accounts for (found to be insignificant) self-sputtering and re-deposition explaining no more than 30% reduction to the utilized also by this code Eckstein's yields. Still, the experimental results are 5–9 times smaller. Fluence was about $3.2 \times 10^{25} \text{ cm}^{-2}$ in all cases.

Case NN	E_{in} [eV]	Exposure time [s]	Eckstein yield	ERO yield	Experimental yield	ERO / Experiment
1	37	1000	1.78×10^{-2}	1.38×10^{-2}	2.84×10^{-3}	5
2	93	550	9.12×10^{-2}	6.21×10^{-2}	7.04×10^{-3}	9
3	92	500	9.05×10^{-2}	5.90×10^{-2}	7.34×10^{-3}	8

comparison with experiment for the BeI 457 nm line for all conditions (Table 1). The singlet line intensity is not that much influenced by the MS tracking as the triplet one, however also for singlets the agreement with the experiment improves. One can see that the dependence on target biasing is reproduced well for conditions “C2” and “C3”. The agreement for “C1” is not that perfect but also good. The effect of plasma conditions is reproduced as well. The absolute values are overestimated in ERO simulations by a factor of about 2, which is however constant for all considered conditions.

The bottom part of Fig. 5 shows the dependence on the cut-off angle. Obviously the focussing of the initial velocity distribution along the PISCES-B axis leads to less side losses and more Be light. It increases the fraction of BeI light and changes the shape of profiles – they go deeper into the plasma. The possible reasons for the COA effect are discussed in Section 4.

4. Mass loss results and discussion

For the spectroscopic observations discussed in the previous section, the clamping ring (also from Be) was included into the ERO simulations to account for the common ring and target surface

(re-)erosion, reflection and re-deposition. However, the mass loss measurements were performed only for the sample with 11 mm radius. The corresponding experimental and simulated results are compared in the Table 2. The exposure time was varied in the experiment in the range 500–1000 s to keep the target fluence constant.

One can see that ERO accounting for net erosion and self-sputtering (much less significant in this particular case) along the target surface helps to come somewhat closer to the experimental results. However, the deviations are too high to be explained by this kind of ERO modeling with any assumptions. In fact ERO simulations based on Eckstein fitting formula applied to every surface cell deviate from the Eckstein value for the characteristic E_{imp} up to ~30%, whereas weight loss indicates factor 5–9 difference with ERO and even larger with the Eckstein fit applied to the E_{imp} in the centre of the target. It should be noted that sputtering yields which are systematically smaller by about an order of magnitude than SDTrimSP data are not a new result [18]: it seems to be rather a rule for the sputtering by small mass species like H, D and He [23].

Returning back to the spectroscopy, ERO simulations show that Eckstein's yields also seem to be overestimated by a factor of 2

or may be even more due to the uncertainty in the COA. The real yield seems to be proportional to the Eckstein fit $Y(0, E_{in})$ with a diminishing factor. This indicates that probably the physical sputtering itself happens in a similar way, so that the BCA simulations remain relevant. Another option is that the reduction occurs due to the prompt processes just after the sputtering.

The latter allows some speculating about the possible reasons behind the COA effect. It is a usual observation at PISCES-B that the initial profiles, just after switching on the plasma, are shorter. The penetration depths rise significantly during the first minutes of the plasma exposure. It was shown earlier that this process is correlated with the growth of multiple cone-like structures on the surface [21,22]. It is easy to imagine that these very steep structures collimate the beam of the eroded particles. They also affect the angle of incidence which would be normal for a flat surface, however it can become very shallow for a cone side. The deeper understanding of these surface morphology issues is not available for now. The most suitable for the purpose MD simulations do not allow including even a single cone, not speaking about a group of those, into the simulation box, which size is limited by the issue of realistic simulation times; the construction of a He-Be potential for MD has also been found nontrivial and is just ongoing [20]. For the present study it is sufficient that this speculation allows considering the COA as an uncertainty.

It should be noted that a proportional but yet diminished yields were observed also for the erosion in D plasma ('ERO-min' fit) [6]. This effect was successfully simulated by MD and to certain extent by BCA approaches both with an assumption of large D content in the PFC surface interaction layer. These data were benchmarked at PISCES-B [19] and JET [7], though in both cases some uncertainty was coming from the molecular release. Further investigation of chemically assisted sputtering (including the experiments in which it is suppressed by the surface temperature) is ongoing.

Both spectroscopy and weight loss approaches indicate the overestimation of the BCA physical sputtering yields. However, spectroscopy gives a much smaller reduction factor of about ~ 2 – 4 , whereas mass loss ~ 5 – 9 makes the methods agree within a factor of 2.5. Partially it can be explained by the remaining uncertainties in both approaches. Still, it is important to note that spectroscopy is characteristic for the gross erosion and the weight loss rather for the net erosion. ERO simulations do not show significant difference between the net and gross erosion (Be re-deposition rates simulated by ERO for conditions discussed in the paper were just 10–30% in relation to the gross erosion), however it may mean that not all related physics is included [1], for instance the effect of the surface roughness which can change local erosion/deposition balance on a microscopic scale. While spectroscopy is quite proportional to the Eckstein's fit, the deviation factor for mass loss measurements (Table 2) is quite scattered. This indicates either large error bars or some unaccounted effect. It is clear that until the surface effects on atomistic level including the nano-level morphology are not understood, it is necessary to continue the gathering of the experimental facts with systematic modeling interpretation: the ERO modeling of similar experiment in D plasma is ongoing, Ar plasma irradiation experiments at PISCES-B are proposed [23].

5. Conclusion

The physical erosion of Be by He plasma in PISCES-B was characterized by spectroscopy and weight loss measurements with interpretation by the PSI and local transport ERO code. Both methods indicate that the Eckstein'2007 [14] fit for the sputtering yields based on SDTrimSP code simulations in BCA approximation overestimate the sputtering yield.

The simulation of axial intensity profiles and their ratios for Be and BeI proves the feasibility of the simulations and the underly-

ing ADAS [16] atomic data. The spectroscopy simulated by ERO deviates by factor 2–4 and reproduces very well the observed trends of the absolute intensities during the plasma parameter and target biasing (sputtering ion impact energy) scan. The uncertainty of about a factor of 2 is associated with the COA in the angle distribution of sputtered ions which is probably related to the changes in the surface morphology (cone-like structures) due to the He plasma irradiation. The MS tracking [17] has somewhat improved the results. A remarkable fact is that the initial population just after sputtering was found to be $MS:GS = 0.33$ independent of plasma conditions and target biasing.

The weight loss results confirm an overestimation of the Eckstein'2007 yields, however the deviation factor is scattered ~ 5 – 9 without a clear trend, which can partially be explained by quite large error bars in these measurements, which are difficult to assess as way are determined not just by the waiting accuracy but for instance due to a possible effect of the shaped clamping ring holding the target. Still, it is difficult to imagine that the net erosion can be underestimated by more than a factor of 2.

It is obvious that further progress demands a deeper understanding of the erosion processes on the atomistic level, including the influence of surface morphology evolution by plasma exposure, e.g. using MD simulations [13]. Further similar experiments (e.g. Be in D and Ar plasma) accompanied by the ERO modeling interpretation can be useful to understand the effects on a phenomenological level.

Acknowledgment

The authors are deeply thankful to Dr Klaus Schmid for a valuable consultation concerning the angular distributions of sputtered particles and to Dr Thomas Schwarz-Selinger for his insight on the light ions sputtering and ideas concerning the further investigations.

The simulation time on JURECA is provided by the Juelich supercomputing centre (JSC).

The work is supported by the EUROfusion WP PFC.

This work has been carried out within the framework of the EUROfusion Consortium and has received funding from the Euratom research and training programme 2014–2018 under grant agreement No 633053. The views and opinions expressed herein do not necessarily reflect those of the European Commission.

References

- [1] R.P. Doerner, et al., Nucl. Fus. 52 (2012) 103003.
- [2] S. Carpentier, et al., J. Nucl. Mat. 415 (2011) S165–S169.
- [3] R.A. Pitts, et al., J. Nucl. Mat. 313–316 (2003) 777–786.
- [4] D. Borodin, et al., Phys. Scr. (2011) 014008 T145.
- [5] A. Kirschner, J.Nucl.Mat. 363–365 (2007) 91–95.
- [6] D. Borodin, et al., J. Nucl. Mat. 438 (2013) S267–S271.
- [7] D. Borodin, et al., Nucl. Mater. Energy 9 (2016) 604–609, doi:10.1016/j.nme.2016.08.013.
- [8] C.C. Klepper, et al., Phys. Scr. (2016) 014035 T167.
- [9] D. Nishijima, et al., J. Nucl. Mater. 463 (2015) 440–444.
- [10] D. Borodin, et al., Contrib. Plasma Phys. 50 (3–5) (2010) 432–438.
- [11] I. Borodkina, et al., Nucl. Mater. Energy (2017), doi:10.1016/j.nme.2017.03.031.
- [12] A. Eksaeva, et al., Nucl. Mater. Energy (2017), doi:10.1016/j.nme.2017.03.014.
- [13] C. Björkas, et al., J. Nucl. Mat. 438 (2013) S276–S279.
- [14] W. Eckstein, Top. Appl. Phys. 110 (2007) 33–187.
- [15] B. LaBombard, et al., J. Nucl. Mater. 162–164 (1989) 314.
- [16] H.P. Summers, The ADAS user manual version 2.6, 2004. <http://adas.phys.strath.ac.uk>.
- [17] D. Borodin, et al., in: 36th EPS Conference on Plasma Phys. Sofia, 2009 ECA, 33, 2009, p. 5.197. E.
- [18] R.P. Doerner, J. Nucl. Mat. 438 (2013) S272–S275.
- [19] C. Björkas, et al., Plasma Phys. Control. Fus. 55 (2013) 074004.
- [20] C. Björkas and K. Nordlund, private communications.
- [21] R.P. Doerner, Phys. Scr. (2014) 014040 T159.
- [22] A. Kreter, et al., Phys. Scr. (2014) 014039 T159.
- [23] T. Schwarz-Selinger, private communications.
- [24] S. Brezinsek, et al., Nucl. Fusion 55 (2015) 063021 T159.